

Dual nature of improper ferroelectricity in a magnetoelectric multiferroic

Silvia Picozzi, Kunihiro Yamauchi

Consiglio Nazionale delle Ricerche - Istituto Nazionale di Fisica della Materia (CNR-INFM), CASTI Regional Lab., 67010 L'Aquila, Italy

Biplab Sanyal

Theoretical Magnetism Group, Department of Physics, Uppsala University, Box-530, SE-75121, Sweden

Ivan A. Sergienko and Elbio Dagotto

Materials Science & Technology Division, Oak Ridge National Laboratory, Oak Ridge, TN 37831, USA and Dept. of Physics, The University of Tennessee, Knoxville, TN 37996, USA

(Dated: March 27, 2019)

One of the fundamental problems in the field of improper magnetic ferroelectrics^{1,2} is the understanding of the microscopic origin of the electric polarization. So far, this question has not been answered experimentally due to very small values of the polarization found in this class of multiferroics^{1,3,4,5}. Here, using first principles calculations, we study the electric polarization in the orthorhombic perovskite manganite HoMnO₃ induced by the antiferromagnetic E-type collinear magnetic structure. We find that a large part of the polarization arises due to the quantum-mechanical effect of electron orbital polarization in addition to the conventional polar atomic displacements. Furthermore, in HoMnO₃ we obtain the largest ferroelectric polarization observed in the whole class of improper magnetic ferroelectrics to date. Finally, a mechanism for switching the magnetoelectric domains via a 180° coherent rotation of Mn spins by the electric field is proposed. To our knowledge, this is the first *ab-initio* study of a material which owes its ferroelectricity to a symmetry breaking induced by magnetic order.

Due to the small size of the Ho ionic radius, HoMnO₃ in its orthorhombic phase (space group *Pnma*) shows⁶ a highly distorted perovskite structure with the Mn-O-Mn *ac*-plane angle $\alpha_0 \approx 144^\circ$. Previous experimental⁷, model^{8,9}, and first-principles¹⁰ reports suggested that this strong distortion leads to the stabilization of the peculiar antiferromagnetic (AFM) E-type spin-alignment, where ferromagnetic zigzag spin-chains in the MnO₂ planes are antiferromagnetically coupled with respect to both adjacent in-plane chains (see Fig. 1a) and out-of-plane stacked chains. The AFM-E phase was indeed observed by neutron scattering⁷ in HoMnO₃ below $T \approx 26$ K. A recent model Hamiltonian study² proposed that AFM-E allows for a ferroelectric polarization along the *c*-axis, whose predicted value $P = 0.5 - 12 \mu\text{C}/\text{cm}^2$ is much higher than that in other improper magnetic ferroelectrics found so far (such as TbMnO₃ or TbMn₂O₅ with $P < 0.1 \mu\text{C}/\text{cm}^2$)^{3,4}. Subsequently, ferroelectricity in HoMnO₃ was observed by Lorenz et al.¹¹ The evi-

dence of ferroelectricity was obtained by pyroelectric current measurements on bulk polycrystalline samples and the observed $P < 2 \text{ nC}/\text{cm}^2$ was three orders of magnitude smaller than the predicted values. Our density functional calculations, complemented by the explicit inclusion of electron-electron correlations in the framework of the GGA+U approximation, allow us to directly address this discrepancy.

In our calculations, we impose the AFM-E order and relax the atomic coordinates. With the optimized atomic positions, the polarization P calculated by the point charge model (PCM) with nominal charges is shown in Fig. 2 as a function of the Hubbard parameter U . P is a decreasing function of U , which is consistent with the general ideas of the model calculations². In that model, the polarization appears due to the difference ($\alpha_p - \alpha_{ap}$) between the Mn-O-Mn angles corresponding to the bonds with parallel (α_p) and antiparallel (α_{ap}) spins, which is a consequence of the Hund's coupling and virtual electronic hopping. In turn, U characterizes the energy penalty paid for adding an additional electron on a Mn site. Thus, increasing U makes the virtual electron hopping less favourable, which reduces $\alpha_p - \alpha_{ap}$ and, ultimately, P . Nevertheless, as shown in Fig. 2, the effect of even a very large $U = 8 \text{ eV}$ is to decrease P by less than half an order of magnitude. As the value of U for HoMnO₃ is not known from experiments, we will resort to a parameter-free density functional treatment with $U = 0$ case from now onwards, noting that the calculated quantities should be trusted at least with respect to their orders of magnitude.

A close look at the geometrically optimized structure in the AFM-E phase reveals a complicated picture of displacements that is shown in Fig. 1b. The Mn atoms displace by 0.04 Å with respect to the initial centrosymmetric *Pnma* structure. The *a* and *b* components of these displacements of different Mn atoms compensate each other, whereas the *c* components add up to a net displacement of 0.01 Å per Mn atom along the negative direction of the *c*-axis. Similarly, the in-plane O atoms are displaced on average by 0.02 Å with the resulting *c*-axis displacement of 0.01 Å per atom in the positive direction. Taking into account relatively smaller

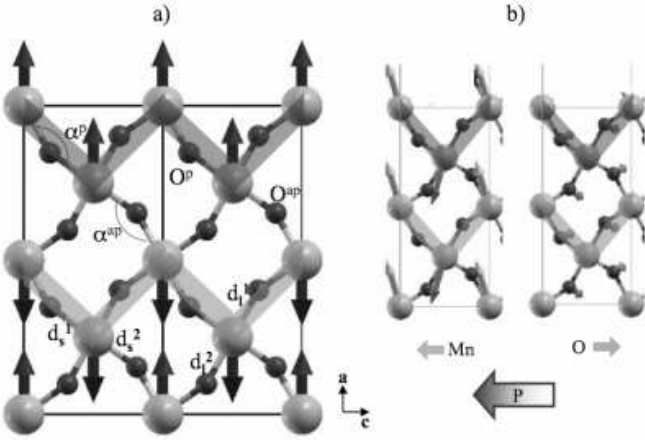


FIG. 1: a) The in-plane arrangement of Mn and O atoms. Arrows denote the direction of spins and antiferromagnetically-coupled zig-zag spin-chains are highlighted by pink and blue shaded areas. Structural parameters reported in Table I are shown. b) Arrows show the directions of the in-plane ionic displacements for Mn (left) and O (right) in the AFM-E phase. The thick arrows at the bottom show the direction of the resulting displacements the Mn and O sublattices and \mathbf{P} .

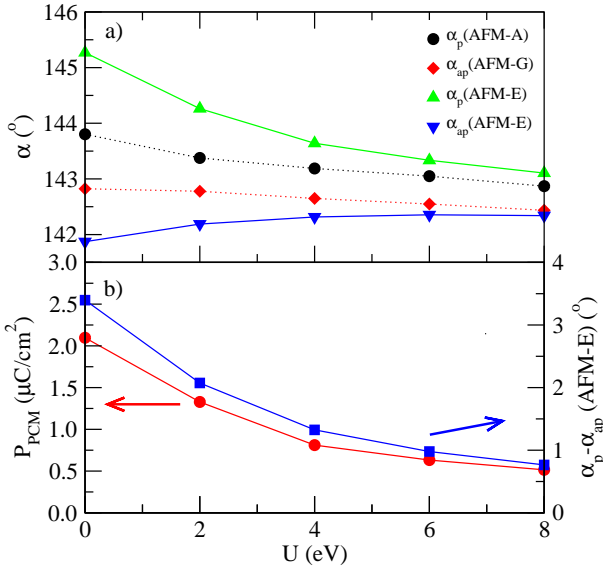


FIG. 2: a) Mn-O-Mn angles (in degrees) in the parallel (α_p) and antiparallel (α_{ap}) Mn spin configurations vs. the Hubbard parameter U . b) Polarization calculated by the point charge model and $\alpha_p - \alpha_{ap}$ in the AFM-E phase.

c -axis displacements of interplane O and Ho atoms we obtain $P_{PCM} = 2.1 \mu\text{C}/\text{cm}^2$. Therefore, our calculations with no fitting parameters independently confirm the large electric polarization obtained in the previous model². In this regard, we hope that the experimentally attained polarization could be improved substantially as it was accomplished for another promising multiferroic BiFeO₃^{12,13}.

To have a better understanding of the structural dis-

TABLE I: Relevant structural parameters for the AFM-A, G and E spin configurations: Mn-O-Mn angle (in degrees) for parallel (α_p) and anti-parallel (α_{ap}) Mn spins, large (d_l^1 and d_l^2) and small (d_s^1 and d_s^2) Mn-O bond-lengths (in Å).

	α_p	α_{ap}	d_l^1	d_l^2	d_s^1	d_s^2
AFM-A	143.8	-	2.20	2.20	1.93	1.93
AFM-G	-	142.8	2.24	2.24	1.90	1.90
AFM-E	145.3	141.9	2.25	2.18	1.92	1.92

tortions caused by the magnetic order, we also optimize the structural parameters for the paraelectric AFM-A (all spins in the ac -plane are parallel) and AFM-G (all neighbouring spins are antiparallel) phases and compare them to the AFM-E structure (see Table I). In agreement with the above discussion, the calculated α_p for AFM-A is larger than α_{ap} for AFM-G. However, when both types of bonds (parallel and antiparallel) are present in the AFM-E phase, this difference is even more pronounced, which explains the relatively high P . In addition, the U -dependence of the angles is shown in Fig. 2a.

The AFM-E phase shows two different kinds of antiferromagnetic domains², E_1 and E_2 (see the left and right insets of Fig. 3a, respectively), which are expected to show opposite polarization, $-P_c$ and P_c . In our calculational unit cell, E_1 and E_2 differ in the orientation of half of the spins (see grey highlighted regions in the central inset). Here, we consider a ferroelectric-AFM switching path from $-P_c$ (E_1) to P_c (E_2) via a progressive rotation of the central spins. According to the basic displacement-like mechanism for polarization, we expect the polarization to switch from negative (in E_1) to positive (in E_2) and to vanish when the relative orientation of the central spins with respect to the fixed spins is close to 90° . The 90° spin-configuration denoted as \perp is shown in the central inset of Fig. 3a. More precisely, \perp is an example of a spiral magnetic structure similar to that in TbMnO₃, but commensurate with the modulation vector $\mathbf{k} = (1/2, 0, 0)$, and which should be ferroelectric with \mathbf{P}_\perp along the c -axis^{14,15,16,17}. As we show in Supplementary Information based on the macroscopic symmetry considerations, the components of the polarization vector \mathbf{P} can be expressed as follows,

$$P_c = \chi_z(c_{xz} \sin \phi - c_0 \cos \phi), \quad P_a = c'_{xz} \chi_x \sin \phi, \quad P_b = 0$$

where χ_x and χ_z are the components of the dielectric susceptibility along the a and c -axes, respectively, and ϕ is the rotation angle of the central spins. The coefficient c_0 stems from nonrelativistic interactions, while c_{xz} and c'_{xz} originate from the coupling of P to the product of the a and c components of the Mn spins, which has a relativistic origin.

The above formulas for \mathbf{P} lead to several important conclusions. First, for the commensurate spiral state \perp ($\phi = \pi/2$), a longitudinal component P_a of the uniform polarization is present in addition to P_c . Second, P_\perp is finite due to purely relativistic effects, in agreement with

previous microscopic models^{14,15}. Third, since the relatively small relativistic effects such as spin orbit coupling are neglected in our computations, we observe that only the c component of the calculated \mathbf{P} is finite for all ϕ and $P \propto \cos \phi$, in excellent agreement with Fig. 3b, which is discussed below. Also, in our computations $P_{\perp} = 0$, and \perp is taken as the reference paraelectric structure with centrosymmetric positions (csp).

If ferroelectric switching is to occur, as the spin rotation proceeds starting from E_1 , the total energy is expected to increase up to a maximum corresponding to the “paraelectric” state (\perp), and then to decrease again until the E_2 minimum is reached. Indeed, this happens when we perform the non-collinear calculations by varying ϕ between 0 and 180° with the full optimizations of the internal atomic coordinates for each spin configuration. The calculated total energy of the system as a function of ϕ (see Fig.3 a) clearly shows a double-well structure, with the depth of the well of about 8 meV/formula unit (f.u.). Although the exact magnitude of the depth of the well can be affected by computational details and approximations, we expect the feasibility of the magnetoelectric switching by the application of realistic electric fields. The calculated energy barrier is smaller than in proper ferroelectric BaTiO₃ (18 meV/f.u.) and PbTiO₃ (200 meV/f.u.), and multiferroic BaMF₄ (> 20 meV/f.u.)^{18,19}.

The evaluation of P deserves a careful discussion, since it leads to intriguing outcome. In Fig.3b, we report the polarization evaluated by the PCM and Berry-phase (BP) approaches within the density-functional-theory (DFT-BP) along the previously mentioned switching path. There is a marked disagreement between the PCM and DFT-BP approaches, therefore suggesting that purely quantum electronic effects are at play in determining the final P , similar to the conventional ferroelectrics²⁰. The idea that P might arise from a purely electronic origin in spiral magnets due to spin orbit coupling was put forward by Katsura *et al.*¹⁴. It was later developed to include collinear multiferroics, for which relativistic effects are not essential²¹. To investigate the purely electronic effects, we calculate the polarization considering the atomic positions of the \perp structure and artificially switching the spin-configuration, without relaxing the lattice degrees of freedom. In this case, due to structural centrosymmetry, there is no contribution from atomic displacements. However, the calculated BP polarization is found to be up to 3.5 $\mu\text{C}/\text{cm}^2$ (see pink triangles in Fig. 3). This large contribution arises solely from the electronic contribution due to symmetry breaking by the AFM-E ordering.

The quantum effects can be quantified further by considering the deviations of the effective Born charges from their nominal valencies. In the \perp case, when each O is coordinated to two Mn atoms with perpendicular spins, we obtain $Z_{\perp}^*(\text{Mn}) = 3.9e$ and $Z_{\perp}^*(\text{O}) = -3.1e$. Along the AFM-FE switching path, the O ions O^p and O^{ap} become increasingly different and acquire different Born

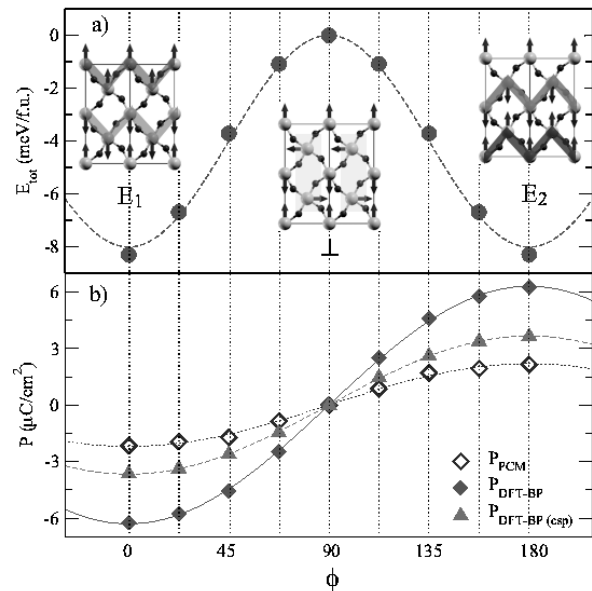


FIG. 3: a) Total energy as a function of the orientation of the central spins (see gray highlighted regions in the central \perp spin-configuration) with respect to the spin of the Mn in the origin. b) Polarization calculated via the PCM (empty blue diamonds) and quantum-mechanically via DFT-BP (filled red diamonds). The pink triangle denotes the values obtained via the DFT-BP approach for centrosymmetric atomic configurations as explained in the text. The lines are fits to $P \propto -\cos \phi$ with constant coefficients.

charges due to the orientation of the Mn spins to which they are bonded. In the extreme points corresponding to AFM-E1 and AFM-E2, we obtain: $Z^*(\text{Mn}) = 3.8e$, $Z^*(\text{O}^a) = -2.6e$ and $Z^*(\text{O}^{ap}) = -3.5e$. Note, that in both \perp and E-type spin arrangements, the Born charges are not extremely different from their nominal valence, consistent with a rather ionic nature of the chemical bonds. We note that the two different kinds of O ions are responsible for ferroelectricity in the case of centrosymmetric positions, where the displacement mechanism is switched off. When atomic relaxation is allowed, all the atoms (including displaced Mn) contribute to the final ferroelectric polarization. The inequivalence of O^a and O^{ap} is further confirmed by the charge density for the fully-relaxed structure, corresponding to the energy range of hybridized Mn e_g and O p orbitals located just below the valence band maximum, as shown in Fig. 4. In addition to the expected G-like orbital ordering^{7,8}, Fig.4 clearly demonstrates that there is a strong asymmetry in the charge distribution between the two O ions. Moreover, focusing on O^{ap} , the charge seems to favor the short Mn-O bond compared to the long bond. This suggests that the polar charge distribution and related wave-functions are due to a delicate combination of the Jahn-Teller effect and symmetry-breaking magnetic ordering.

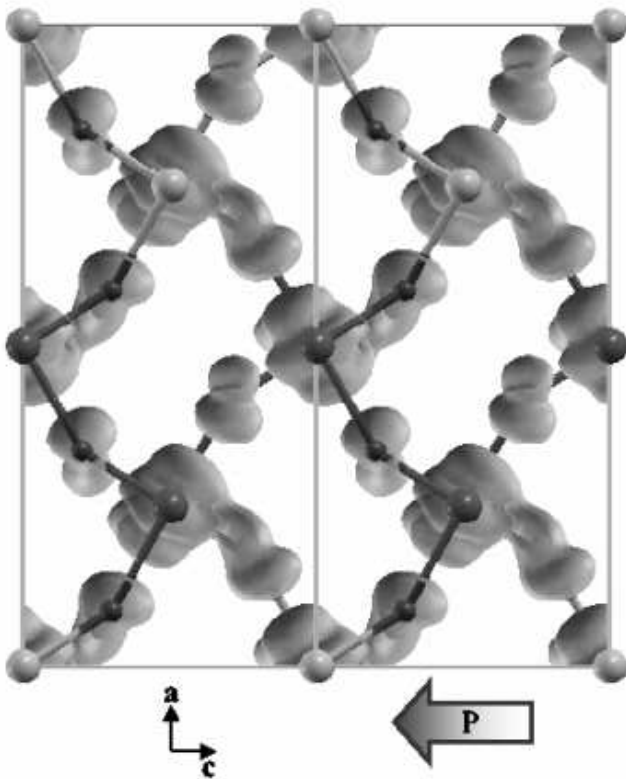


FIG. 4: The ac -plane charge density isosurface plot in the energy range $[-0.8:0]$ eV (considering the top of the valence band as zero of the energy scale) for fully relaxed positions in the AFM-E1 spin configuration. Blue (green) balls denote Mn atoms with up (down) spins.

In summary, our first-principles results show that, in the antiferromagnetic E-type HoMnO_3 , the symmetry-induced inequivalence of the in-plane Mn-O-Mn configurations for parallel and antiparallel spins is an efficient mechanism in driving a considerable ferroelectric polarization. The calculated total polarization of the AFM-E phase, $P \approx 6\mu\text{C}/\text{cm}^2$ is consistent with the previously obtained theoretical estimates². In addition to the displacement mechanism, we find a larger but comparable

contribution arising from a purely electronic quantum effect of orbital polarization. The finite ferroelectric polarization, even with a centrosymmetric atomic arrangement, is an unambiguous indication of a magnetism-induced electronic mechanism at play. Also, a magneto-electric domain switching path is proposed, in which the reversal of polarity of the applied electric field induces a 180° -flip of selected spins.

Methods. First-principles calculations based on the generalized gradient approximation²² to density functional theory have been performed using the Vienna Ab-initio Simulation Package (VASP)²³ and the projector-augmented-wave pseudopotentials.²⁴ Ho $4f$ electrons were assumed as frozen in the core and therefore do not play any role in the present context. The plane wave energy cut-off was set to 500 (400) eV for the collinear (non-collinear) calculations. The Brillouin zone sampling was performed using the $3 \times 4 \times 6$ shell according to the Monkhorst-Pack algorithm.²⁵ The GGA+U²⁶ calculations were performed by applying a Hubbard-like potential for Mn d states. U was varied in the range from 0 to 8 eV; accordingly, we chose $J = 0.15 \cdot U$. The Berry phase approach^{27,28} was used to calculate the polarization, integrating over six \mathbf{k} -point strings parallel to the c axis, each string containing 6 \mathbf{k} -points. Non-collinear calculations were performed according to the formalism reported in Ref.29. Spin-orbit coupling was neglected. As for the structural details, we chose the experimental lattice constants⁶ for HoMnO_3 for the orthorhombic unit-cell ($a = 5.835 \text{ \AA}$, $b = 7.361 \text{ \AA}$ and $c = 5.257 \text{ \AA}$) and performed atomic relaxations until the Hellman-Feynman forces were below 0.015 eV/\AA .

Acknowledgements. Simulations have been performed on supercomputer MareNostrum at Barcelona Supercomputing Center. We also appreciate computational support from Swedish National Infrastructure for Computing (SNIC). Research at ORNL is sponsored by the Division of Materials Sciences and Engineering, Office of Basic Energy Sciences, U.S. Department of Energy, under Contract No. DE-AC05-00OR22725 with Oak Ridge National Laboratory, managed and operated by UT-Battelle, LLC. I.S. is supported in part by NSF Grant No. DMR-0072998. I.S. and E.D. are supported in part by NSF Grant No. DMR-0443144.

1. Cheong S.-W. & Mostovoy M. Multiferroics: a magnetic twist for ferroelectricity. *Nature Mater.* **6**, 13-20 (2007).
2. Sergienko I.A., Şen C. & Dagotto E. Ferroelectricity in the Magnetic E-phase of Orthorhombic Perovskites. *Phys. Rev. Lett.* **97**, 227204 (2006).
3. Kimura T., Goto T., Shintani H., Ishizaka K., Arima T., and Tokura Y. Magnetic control of ferroelectric polarization. *Nature* **426**, 55-58 (2003).
4. Hur N., Park S., Sharma P.A., Ahn J.S., Guha S., and Cheong S.-W. Electric polarization reversal and memory in a multiferroic material induced by magnetic fields. *Nature* **429**, 392-395 (2004).
5. Aliouane N., Argyriou D.N., Stremper J., Zegkinoglou

- I., Landsgesell S., Zimmermann M., Field-induced linear magnetoelastic coupling in multiferroic TbMnO_3 . *Phys. Rev. B* **73**, 020102(R) (2006).
6. Alonso A.J., Martínez-Lope M.J., Casais M.T., Fernández-Díaz M.T. Evolution of the Jahn-Teller distortion of MnO_6 octahedra in RMnO_3 perovskites (R = Pr, Nd, Dy, Tb, Ho, Er, Y): A Neutron Diffraction Study. *Inorg. Chem.* **39**, 917-923 (2000).
7. Muñoz A., Casáis M.T., Alonso J.A., Martínez-Lope M.J., Martínez J.L., and Fernández-Díaz M.T. Complex Magnetism and Magnetic Structures of the Metastable HoMnO_3 Perovskite. *Inorg. Chem.* **40**, 1020-1028 (2001).
8. Hotta T., Moraghebi M., Feiguin A., Moreo A., Yunoki

- S., Dagotto E., Unveiling new magnetic phases of undoped and doped manganites. *Phys. Rev. Lett.***90**, 247203 (2003).
9. Kimura T., Ishihara S., Shintani H., Arima T., Takahashi K.T., Ishizaka K., and Tokura Y. Distorted perovskite with e_g^1 configuration as a frustrated spin system. *Phys. Rev. B* **68**, 060403(R) (2003).
 10. Picozzi S., Yamauchi K., Bihlmayer G. and Bluegel S. First principles stabilization of an unconventional collinear magnetic ordering in distorted manganites. *Phys. Rev. B* **74**, 094402 (2006).
 11. Lorenz B., Wang Y.Q., and Chu C.W. Ferroelectricity in perovskite HoMnO_3 and YMnO_3 . cond-mat/0608195.
 12. Neaton J.B., Ederer C., Waghmare U.V., Spaldin N.A., and Rabe K.M. First-principles study of spontaneous polarization in multiferroic BiFeO_3 . *Phys. Rev. B***71**, 014113 (2005).
 13. Ramesh R. and Spaldin N.A. Multiferroics: progress and prospects in thin films. *Nature Mater.* **6**, 21-29 (2007).
 14. Katsura H., Nagaosa N., Balatsky A. V. Spin Current and Magnetoelectric effect in non-collinear magnets. *Phys. Rev. Lett.***95**, 057205 (2005).
 15. Sergienko I.A. and Dagotto E. Role of the Dzyaloshinskii-Moriya interaction in multiferroic perovskites. *Phys. Rev. B* **73**, 094434 (2006).
 16. Kenzelmann M., Harris A.B., Jonas S., Broholm C., Schefer J., Kim S.B., Zhang C. L., Cheong S.W., Vajk O.P. & Lynn W.J. Magnetic inversion symmetry breaking and ferroelectricity in TbMnO_3 . *Phys. Rev. Lett.***95**, 087206 (2006).
 17. Mostovoy M. Ferroelectricity in Spiral Magnets. *Phys. Rev. Lett.* **96**, 067601 (2006).
 18. Cohen R. E. Origin of ferroelectricity in perovskite oxides. *Nature* **358**, 136 - 138 (1992).
 19. Ederer C. and Spaldin N. A. Origin of ferroelectricity in the multiferroic barium fluorides BaMF_4 : A first principles study. *Phys. Rev. B* **74**, 024102 (2006).
 20. Zhong W., King-Smith R.D., and Vanderbilt D. Giant LO-TO Splittings in Perovskite Ferroelectrics, *Phys. Rev. Lett.* **72**, 3618-3621 (1994).
 21. Jia C., Onoda S., Nagaosa N., and Han J.H. Spin-polarization coupling in multiferroic transition-metal oxides. cond-mat/0701614.
 22. Perdew J.P., Burke K., and Ernzerhof M. Generalized Gradient Approximation made simple. *Phys. Rev. Lett.***77**, 3865-3868 (1996)
 23. Kresse G. and Furthmüller J. Efficient iterative schemes for ab-initio total energy calculations using a plane-wave basis set. *Phys. Rev. B***54**, 11169-11186 (1996).
 24. Kresse G. and Joubert G. From ultrasoft pseudopotentials to the projector augmented-wave method. *Phys. Rev. B***59**, 1758-1775 (1999).
 25. Monkhorst H.J. and Pack J.D. Special points for Brillouin zone integrations. *Phys. Rev. B***13**, 5188-5192 (1976).
 26. Anisimov V.I., Aryasetiawan F. and Lichtenstein A.I. First-principles calculations of the electronic structure and spectra of strongly correlated systems: the LDA+U method. *J. Phys.: Condens. Matter.***9**, 767-808 (1997).
 27. King-Smith R.D. and Vanderbilt D. Theory of polarization of crystalline solids. *Phys. Rev. B***47**, 1651-1654 (1993).
 28. Resta R. Macroscopic polarization in crystalline dielectrics: the geometric phase approach. *Rev. Mod. Phys.***66**, 899-915 (1994).
 29. Hobbs D., Kresse G. and Hafner J. Fully unconstrained non-collinear magnetism within the projector augmented-wave method. *Phys. Rev. B***62**, 11556-11570 (2000).
 30. Landau, L.D. & Lifshitz, E.M. *Statistical Physics, Part I* (Pergamon Press, Oxford, 1980).
 31. Hahn, T. (ed.) *International Tables for Crystallography 5th edn, Vol. A* (Kluwer, Dordrecht, 2002).
 32. Tolédano J.-C. & Tolédano P. *The Landau Theory of Phase Transitions* (World Scientific, Singapore, 1987).

Supplementary Information

Here we give a brief derivation of selected results of the Landau theory theory of phase transitions³⁰ applied to the AFM-E order and its coupling to ferroelectricity. Here we work in the $Pnma$ (#62) space group setting, which is related to $Pbnm$ used in Ref. 2 via a different choice of the orthorhombic axes³¹. We also place the origin in the Mn position. The order parameter of the magnetic ordering ($\mathbf{E}_1, \mathbf{E}_2$) is written as a linear combination of Mn spins \mathbf{S}_i , where $i = 1, \dots, 8$ denotes the Mn atoms occupying the following positions in the magnetic unit cell, corresponding to the modulation vector $\mathbf{k} = (1/2, 0, 0)$:

$$1 : (000), \quad 2 : (\frac{1}{2}0\frac{1}{2}), \quad 3 : (100), \quad 4 : (\frac{3}{2}0\frac{1}{2}), \quad 5 : (0\frac{1}{2}0), \quad 6 : (\frac{1}{2}\frac{1}{2}\frac{1}{2}), \quad 7 : (1\frac{1}{2}0), \quad 8 : (\frac{3}{2}\frac{1}{2}\frac{1}{2}),$$

The order parameter is obtained as²

$$\begin{aligned} \mathbf{E}_1 &= \mathbf{S}_1 - \mathbf{S}_2 - \mathbf{S}_3 + \mathbf{S}_4 - \mathbf{S}_5 + \mathbf{S}_6 + \mathbf{S}_7 - \mathbf{S}_8, \\ \mathbf{E}_2 &= \mathbf{S}_1 + \mathbf{S}_2 - \mathbf{S}_3 - \mathbf{S}_4 - \mathbf{S}_5 - \mathbf{S}_6 + \mathbf{S}_7 + \mathbf{S}_8. \end{aligned} \quad (1)$$

The components of \mathbf{E}_1 and \mathbf{E}_2 transform according to the rules given in Table II, where the transformation rules for electric polarization \mathbf{P} are also summarized. Here, we analyze the possible magnetoelectric coupling terms of the form $\mathbf{P} \cdot \mathbf{E}^2$ in the thermodynamic potential:

$$\begin{aligned} F_{\text{me}} &= c_0 P_z (\mathbf{E}_1^2 - \mathbf{E}_2^2) + c_{yy} P_z (E_1^{y2} - E_2^{y2}) + c_{zz} P_z (E_1^{z2} - E_2^{z2}) + c_{xz} P_z (E_1^x E_2^z - E_2^x E_1^z) + c'_{xz} P_x (E_2^z E_2^x - E_1^z E_1^x) \\ &\quad + d_{xy} P_y (E_1^y E_2^x - E_2^y E_1^x) + d_{zy} P_y (E_1^y E_1^z - E_2^y E_2^z). \end{aligned} \quad (2)$$

Clearly, only the first term has a nonrelativistic origin since $(\mathbf{E}_1^2 - \mathbf{E}_2^2)$ is a linear combination of the terms $(\mathbf{S}_i \cdot \mathbf{S}_k)$.

Considering Eq. (2) together with the usual dielectric energy $F_{\text{de}} = 1/2(\chi_x^{-1} P_x^2 + \chi_y^{-1} P_y^2 + \chi_z^{-1} P_z^2)$, we obtain that $P_y = 0$ if $E_1^y = E_2^y$, which always holds in our case. The other two components of \mathbf{P} are given as

$$P_x = -\chi_x c'_{xz} (E_2^z E_2^x - E_1^z E_1^x), \quad P_z = -\chi_z [c_0 (\mathbf{E}_1^2 - \mathbf{E}_2^2) + c_{zz} (E_1^{z2} - E_2^{z2}) + c_{xz} (E_1^x E_2^z - E_2^x E_1^z)]. \quad (3)$$

As is proposed in the main text, the switching of the magnetoelectric domain is accomplished by rotating the spins $\mathbf{S}_2, \mathbf{S}_4, \mathbf{S}_6$, and \mathbf{S}_8 in the xz -plane. Thus, we set

$$\mathbf{S}_1 = -\mathbf{S}_3 = -\mathbf{S}_5 = \mathbf{S}_7 = S(1, 0, 0), \quad -\mathbf{S}_2 = \mathbf{S}_4 = \mathbf{S}_6 = -\mathbf{S}_8 = S(\cos \phi, 0, \sin \phi),$$

Using Eqs. (1) and (3), it is easy to verify that $\phi = 0$ and $\phi = \pi$ correspond to the domains $E_1^x(-P_z)$ and $E_2^x(+P_z)$, respectively. Furthermore, we obtain,

$$P_x = \chi_x 32 S^2 c'_{xz} \sin \phi, \quad P_z = \chi_z (32 S^2 c_{xz} \sin \phi - 64 S^2 c_0 \cos \phi),$$

which are equivalent to the expressions given in the main text with the numerical constants and S^2 adsorbed in the coefficients.

As a by-product of the present analysis we also find that the following term is allowed in the thermodynamic potential:

$$F_L = \frac{\lambda}{V} \int (E_1^x \partial_x E_2^x - E_2^x \partial_x E_1^x) dV.$$

This *Lifshitz*^{30,32} term leads to the following typical series of phase transition when the temperature is lowered: Para-phase \rightarrow Incommensurate phase \rightarrow ‘‘Locked-in’’ commensurate phase³², which was indeed observed in HoMnO_3 ⁷. It can be shown³² that both E_1^x and E_2^x are modulated with $\mathbf{k}(T) = (1/2 + \delta k(T), 0, 0)$ in the AFM-Incommensurate phase. Taking into account the magnetoelectric interactions (2), this leads to a vanishing macroscopic polarization in the incommensurate phase in agreement with the experiment¹¹.

TABLE II: Matrices of the generators of space group $Pnma$ in the representations spanned by \mathbf{E}_1 , \mathbf{E}_2 , and \mathbf{P} . The space group elements are denoted $(r|hkl)$, where r is the identity operation 1, two-fold rotation $2_{a,c}$, inversion I , or time reversal $1'$ followed by the translation $\boldsymbol{\tau} = h\mathbf{a} + k\mathbf{b} + l\mathbf{c}$.

	$(2_z \frac{1}{2}0\frac{1}{2})$	$(2_y 0\frac{1}{2}0)$	$(I 000)$	$(1 010)$	$(1' 000)$
E_1^x	1 0	0 1	0 1	-1 0	-1 0
E_2^x	0 -1	1 0	1 0	0 -1	0 -1
E_1^y	1 0	0 -1	0 1	-1 0	-1 0
E_2^y	0 -1	-1 0	1 0	0 -1	0 -1
E_1^z	-1 0	0 1	0 1	-1 0	-1 0
E_2^z	0 1	1 0	1 0	0 -1	0 -1
P_x	-1	-1	-1	1	1
P_y	-1	1	-1	1	1
P_z	1	-1	-1	1	1